



OPEN

# Self-Assembly and Horizontal Orientation Growth of VO<sub>2</sub> Nanowires

SUBJECT AREAS:

NANOWIRES

Chun Cheng<sup>1</sup>, Hua Guo<sup>2</sup>, Abbas Amini<sup>3</sup>, Kai Liu<sup>4</sup>, Deyi Fu<sup>4</sup>, Jian Zou<sup>4</sup> & Haisheng Song<sup>5</sup>

SYNTHESIS AND PROCESSING

Received  
7 May 2014Accepted  
9 June 2014Published  
26 June 2014Correspondence and  
requests for materials  
should be addressed to  
C.C. (cheng.c@sustc.  
edu.cn)

<sup>1</sup>Department of Materials Science and Engineering, South University of Science and Technology, Shenzhen 518055, China, <sup>2</sup>National Center for Electron Microscopy, Lawrence Berkeley National Laboratory, Berkeley, CA 94720, USA, <sup>3</sup>School of Computing, Engineering and Mathematics, University of Western Sydney, Kingswood, NSW 2751, Australia, <sup>4</sup>Department of Materials Science and Engineering, University of California, Berkeley, CA 94720, USA, <sup>5</sup>Wuhan National Laboratory for Optoelectronics (WNLO) and the School of Optical and Electronic Information, Huazhong University of Science and Technology, Wuhan 430074, China.

Single-crystalline vanadium dioxide (VO<sub>2</sub>) nanostructures have attracted an intense research interest recently because of their unique single-domain metal-insulator phase transition property. Synthesis of these nanostructures in the past was limited in density, alignment, or single-crystallinity. The assembly of VO<sub>2</sub> nanowires (NWs) is desirable for a “bottom-up” approach to the engineering of intricate structures using nanoscale building blocks. Here, we report the successful synthesis of horizontally aligned VO<sub>2</sub> NWs with a dense growth mode in the [1-100]<sub>quartz</sub> direction of a polished x-cut quartz surface using a simple vapor transport method. Our strategy of controlled growth of VO<sub>2</sub> NWs promisingly paves the way for designing novel metal-insulator transition devices based on VO<sub>2</sub> NWs.

Vanadium dioxide (VO<sub>2</sub>), a representative strongly correlated electron material, is of great interest due to its first-order metal-insulator transition (MIT) at temperatures slightly above room temperature ( $T_C = 68^\circ\text{C}$ , where  $T_C$  is transformation temperature)<sup>1</sup>. This phase transition mainly features a coupled structural—electronic phase transformation from a monoclinic, insulating phase (I) at low temperatures to a rutile, metallic phase (M) at high temperatures. Meanwhile, VO<sub>2</sub> exhibits a drastic change in optical reflectivity across the MIT, as well as a size change of up to 1% and several orders of magnitude drop in resistivity<sup>2</sup>. Exploiting these switching behaviors across the MIT, a number of applications have been demonstrated or proposed in optical switches, smart window coating, Mott transistors, memristors, sensors, and thermal actuators<sup>3,4</sup>. Despite these expanding applications, fundamental challenges still remain for reliable MIT engineering using VO<sub>2</sub>. For instance, the strain associated with grain boundary, dislocation, stoichiometry fluctuation and substrate clamping can broaden the phase transition temperature window<sup>3</sup>. Single-crystal nanowires offer an appealing alternative to thin films because they host single domains across their entire width, and thus support single or few domain MIT<sup>5–8</sup>. Based on this unique single domain MIT characteristic of VO<sub>2</sub> NWs, different aspects of the physics of MIT were discovered<sup>9–11</sup>, and a variety of applications in actuators<sup>5,8</sup>, gas sensors<sup>12</sup>, power meters<sup>6</sup>, and strain gauges<sup>13</sup> were demonstrated. Due to these promising applications, VO<sub>2</sub> NWs have attracted a great interest as building blocks used for the fabrication of nanodevices.

Considerable effort have in recent years been expended to the control of the growth of VO<sub>2</sub> NWs using simple thermal evaporation methods<sup>14–17</sup>. Usually, VO<sub>2</sub> NWs are preferentially grown on substrates such as silicon, oxidized silicon surface, fused quartz, etc., through a vapor-solid (VS) process<sup>17</sup>. They are randomly dispersed and embedded into the substrates. Careful and selective etching is needed to release the VO<sub>2</sub> NWs from the substrates in order to assemble them for the aforementioned applications. This “liberation” process is typically slow with a low-yield and may damage the NWs surface. It is therefore necessary to develop an effective synthesis method of free-standing single-crystal VO<sub>2</sub> NWs with high densities and high aspect ratios. This kind of growth has recently been achieved by our group using rough surface quartz<sup>14</sup>. Other methods that have been explored include: 1) directed and heteroepitaxial growth of VO<sub>2</sub> NWs on special substrates with a certain lattice match of surfaces such as a-cut/c-cut sapphire, c-cut GaN, (110) TiO<sub>2</sub> etc.<sup>15,18</sup> 2) several alternative templating techniques for the control of the position and orientation of VO<sub>2</sub> nanostructures including: (a) surface patterning with precursor powder<sup>16</sup> and (b) templating against a microstructure substrate<sup>15</sup>. However, the efforts that have been expended in this direction suffer from drawbacks such as expensive epitaxial substrates as mentioned above and/or a poor product density. With these shortcomings, the mass production of high-quality and oriented VO<sub>2</sub> NWs still remains a



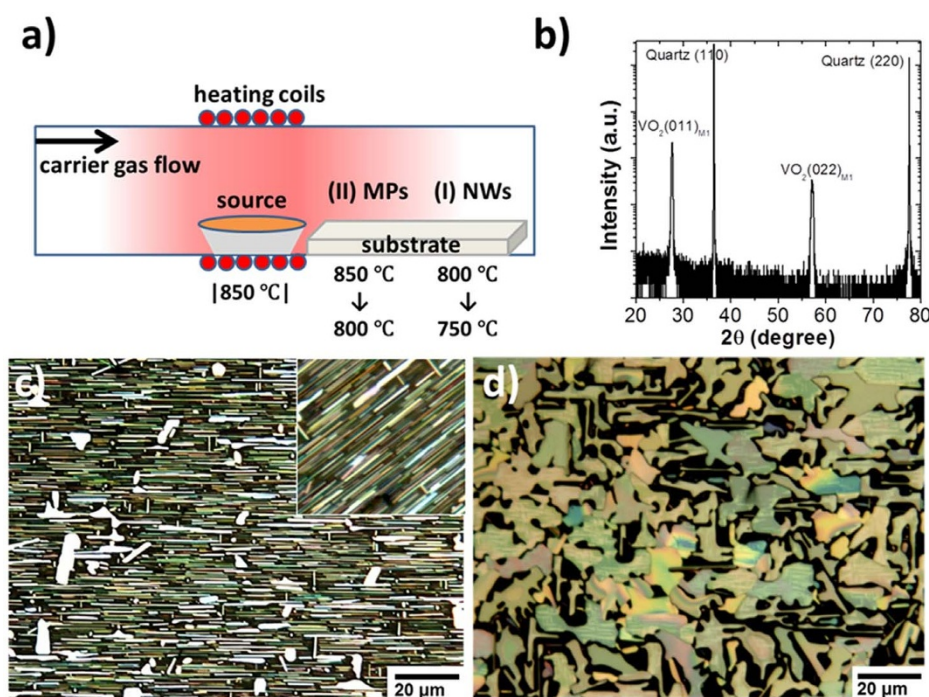
challenge for nanotechnologists. In this work, we present a method to fabricate the ordered arrays of VO<sub>2</sub> NWs in a large scale on relatively inexpensive x-cut quartz substrates.

## Results

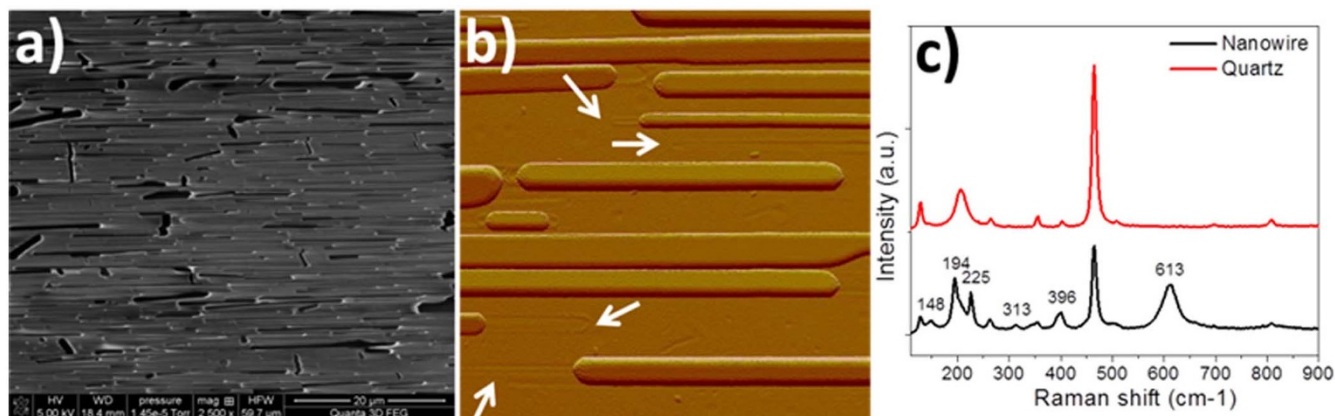
Figure 1a shows a schematic of the reactor setup and the formation temperatures of as-prepared products. Two kinds of morphologies, namely nanowires (NWs) in region I (750–800 °C) and microplates (MPs) in region II (800–850 °C), are observed. Fig. 1b shows a representative XRD spectrum of the products on substrates. The XRD peaks can be indexed to the low-temperature and monoclinic structure of VO<sub>2</sub> (JCPDS card 72-0514). It is noted that besides the (011) and (022) peaks which appear in the in-plane growth of VO<sub>2</sub> NWs, there are no other peaks such as (002), (020), (021), (013), (200), (-212), (-311), (300), *etc.* This fact suggests a preferential orientation of the VO<sub>2</sub> products with the (011) plane parallel to the surface of the quartz substrate which resulted from the epitaxial growth. Figs. 1c and d show the representative optical images of as-grown products. High density VO<sub>2</sub> NWs were the dominating products in the low-temperature deposition zone (I). In contrast with the randomly oriented in-plane growth of VO<sub>2</sub> NWs on other reported substrates, such as silicon, oxidized silicon surface, fused quartz, *etc.*<sup>15</sup>, the present VO<sub>2</sub> NWs only grow along one direction. The diameters of VO<sub>2</sub> NWs normally range from tens to hundreds of nm and their lengths are several tens of micrometers. The diameters and densities of VO<sub>2</sub> NWs are shown to be temperature dependent. Low growth temperatures resulted in small diameters and a low density of VO<sub>2</sub> NWs. High growth temperatures favor the fusing of NWs and enhance their lateral growth leading to an MP morphology as shown in Fig. 1c. The grown embedded VO<sub>2</sub> MPs in the substrates have an irregular shape with a submicrometer thickness and size of tens of micrometer. Rich domain patterns are observed in these VO<sub>2</sub> MPs which can be attributed to the twinning of a low-temperature phase or to the formation of two mixed monoclinic phases<sup>19</sup>. This manifests the existence of the elastic strain induced in the MPs by the substrate upon the following cooling process<sup>20</sup>.

Figure 2a shows a typical SEM image of NW products at the deposition temperature of 800 °C. The image has a weak contrast due to the poor electrical conductivity of VO<sub>2</sub> and the quartz substrate. The NWs density is quite high and they appear to integrate together forming a NW film. Fig. 2b is an AFM image of VO<sub>2</sub> NWs grown at a low deposition temperature of 750 °C. There are two distinct features for the as-grown VO<sub>2</sub> NWs: 1) there is no overlap between two NWs when they meet, that is, one NW growth front is stopped by another NW. 2) There are obvious traces of grooves left aside the two ends of each VO<sub>2</sub> NW due to the dissolution of SiO<sub>2</sub> during the growth process. All the VO<sub>2</sub> NWs are in the monoclinic phase as confirmed by the micro-Raman spectra of nanowires and quartz substrate in Fig. 2c. The Raman spectrum at room temperature shows characteristic vibration modes for the monoclinic insulating phase of VO<sub>2</sub>. Comparing with the previous work on thin films and bulk crystals<sup>21</sup>, the Raman peaks at room temperature are identified as 148(A<sub>g</sub>), 194(A<sub>g</sub>), 225(A<sub>g</sub>), 313(B<sub>g</sub>), 396(A<sub>g</sub>) and 613(A<sub>g</sub>) cm<sup>-1</sup><sup>13</sup>. There are no peaks related to V<sub>2</sub>O<sub>5</sub> and other stoichiometries. This is consistent with our XRD data and following TEM results.

The interface between the root of a single VO<sub>2</sub> nanowire and quartz substrate was investigated by cross-section TEM imaging (see Fig. 3a). The TEM sample was prepared using focus ion beam (FIB) milling with the cross-section plane perpendicular to the VO<sub>2</sub> NW growth direction. The cross-section of VO<sub>2</sub> NW shows a rectangular shape and the VO<sub>2</sub>/quartz interface is flat. Figs. 3b–d show the selected area electron diffraction (SAED) patterns taken from the NW, quartz substrate and the interface, respectively. The SAED pattern P1 was indexed to be monoclinic VO<sub>2</sub>. The diffraction spots were clear and round and the pattern did not change as the electron beam moved along the nanowire indicating that the whole nanowire is a single crystal without stacking faults. The HRTEM image in Fig. 3e taken from the NW shows clear lattice fringes, again confirming the good crystallinity of the NW. The marked lattice spacing of 0.451 nm corresponds to the inter-plane spacing of the (010) and (001) planes of monoclinic VO<sub>2</sub> crystals. From the above SAED



**Figure 1** | (a) Schematic of the tube furnace reactor (not in scale). Temperature of the reactor is shown by red (hot) and white (cold) colors. (b) XRD spectrum of the products. The morphology of the grown products observed in accordance with the distance for: (c) nanowires and (d) microplates. Inset of (a): an enlarged optical image of as-grown VO<sub>2</sub> NWs.



**Figure 2** | (a) SEM image of VO<sub>2</sub> nanowires grown horizontally on the surface of substrate. (b) AFM image of VO<sub>2</sub> nanowires. There are obvious traces of grooves left aside the two ends of each VO<sub>2</sub> NW as marked by the arrows. (c) Raman spectra of the nanowires and quartz substrate. Besides the peaks from quartz, all other peaks are attributed to monoclinic VO<sub>2</sub>.

studies (Figs. 3b–d), the orientation relationships between VO<sub>2</sub> NW and the quartz substrate can be identified as below:

$$(011)_{\text{VO}_2 \text{ monoclinic}} // (11-20)_{\text{quartz}}; [100]_{\text{VO}_2 \text{ monoclinic}} // [1-100]_{\text{quartz}}$$

It is therefore confirmed that the NW is surrounded by {011} faces and its axis is along the [100]<sub>monoclinic</sub> direction. The NW growth direction is aligned with [1-100]<sub>quartz</sub>. During the growth process, the VO<sub>2</sub> phase is rutile. This is because the deposition temperature is higher than  $T_c$  while it changes to the monoclinic phase after cooling to room temperature. Here, it is necessary to study the lattice match relationship between the two phases of VO<sub>2</sub> and the quartz substrate. With regard to this orientation relationship, VO<sub>2</sub> has a good lattice match with the quartz in both the metal rutile and insulator monoclinic phases as shown below:

$1 \times d_{(1000)/\text{quartz}} (0.426 \text{ nm}) \approx 3 \times d_{(002)/\text{VO}_2 \text{ rutile}} (0.428 \text{ nm})$ , the lattice mismatch is 0.5%, the normal directions of these two planes are parallel to  $[1-100]_{\text{quartz}}$ ;

$3 \times d_{(0001)/\text{quartz}} (1.622 \text{ nm}) \approx 5 \times d_{(110)/\text{VO}_2 \text{ rutile}} (1.610 \text{ nm})$ , the lattice mismatch is 0.8%, the normal directions of these two planes are parallel to  $[0001]_{\text{quartz}}$ ;

$1 \times d_{(1000)/\text{quartz}} (0.426 \text{ nm}) \approx 3 \times d_{(-402)/\text{VO}_2 \text{ monoclinic}} (0.430 \text{ nm})$ , the lattice mismatch is 0.9%, the normal directions of these two planes are parallel to  $[1-100]_{\text{quartz}}$ ;

$3 \times d_{(0001)/\text{quartz}} (1.622 \text{ nm}) \approx 5 \times d_{(011)/\text{VO}_2 \text{ monoclinic}} (1.600 \text{ nm})$ , the lattice mismatch is 1.4%, the normal directions of these two planes are parallel to  $[0001]_{\text{quartz}}$ .

The calculated lattice mismatches between rutile VO<sub>2</sub> and quartz are only 0.5% along the  $[1-100]_{\text{quartz}}$  and 0.8% along the  $[0001]_{\text{quartz}}$  direction for the VO<sub>2</sub> rutile phase. It is known that VO<sub>2</sub> NWs have a preferred growth direction along  $[001]_{\text{VO}_2 \text{ rutile}}$ . The above anisotropic lattice mismatch relationships definitely determine the fast growth of VO<sub>2</sub> NW along the  $[1-100]_{\text{quartz}}$  direction due to the best lattice match relationship while the width of NWs along  $[0001]_{\text{quartz}}$  direction is limited due to a larger lattice mismatch. This rationale supports the self-assembled oriented growth of VO<sub>2</sub> NW on x-cut quartz substrate. Similar anisotropic lattice mismatch relationship between quartz and monoclinic phase VO<sub>2</sub> is kept after cooling down to room temperature. In case of VO<sub>2</sub> MPs, the observed linear domain patterns along the  $[1-100]_{\text{quartz}}$  direction (Fig. 1d) can be attributed to the elastic strain caused by the synergistic effect of the large lattice mismatch 0.8%/1.4% (high T/room T) perpendicular to the  $[1-100]_{\text{quartz}}$  direction and the large difference in expansion coefficients between these two crystals (about two orders of magnitude)<sup>18</sup>.

We did not observe horizontally aligned growth of VO<sub>2</sub> NWs on z-cut (0001) quartz. This is a strong indication of the important role of the surface crystallographic plane in determining the direction of NW growth. As such, compared with z-cut (0001) quartz, the x-cut (11-20) quartz is shown to be a superior substrate for VO<sub>2</sub> growth due to the lattice match relationship. A similar growth behavior was found for the horizontal growth of ZnO NWs on x-cut sapphire through a metal-catalyzed vapor-liquid-solid (VLS) growth mechanism<sup>22</sup>. Fig. 4(a) schematically illustrates the growth direction of NWs and the VO<sub>2</sub>  $[001]_{\text{rutile}}$  direction relative to x-cut (11-20) quartz. Fig. 4b proposes a model derived from the SAED results. In this model, the (110) plane of VO<sub>2</sub> rutile is considered parallel to the a-plane of quartz. Only in this arrangement will V atoms (small red circles) have a reasonable overlap with oxygen atoms (large navy blue circles) of quartz. Interestingly, the two crystals appear to have a better match in the  $\pm[1-100]_{\text{quartz}}$  direction which coincides with

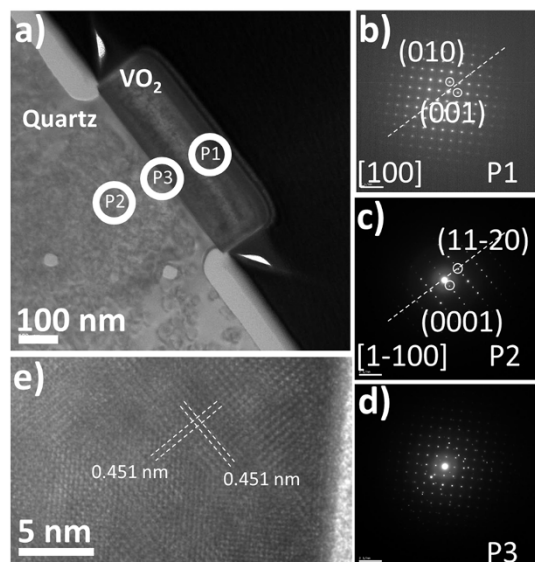


**Figure 3** | (a) TEM image of the cross-section of the interface between a single nanowire and quartz substrate; (b–d) SAED patterns corresponding to the areas marked with P1 (VO<sub>2</sub>), P2 (quartz), P3 (interface). The dash lines in (b) – (c) indicate the normal directions of  $(011)_{\text{VO}_2 \text{ monoclinic}}$  and  $(11-20)_{\text{quartz}}$ . (e) High resolution transmission electron microscopy (HRTEM) image of VO<sub>2</sub> nanowire taken at the  $[100]$  zone axis.

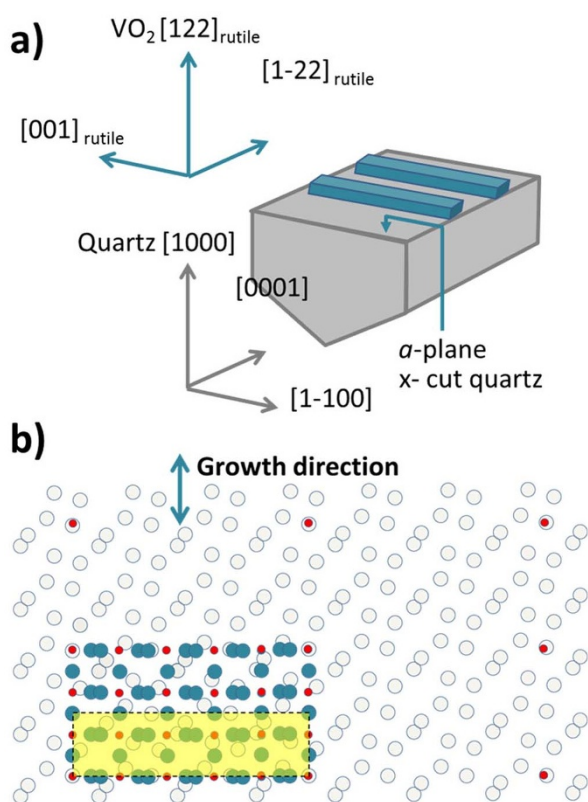


**Figure 4** | (a) The growth direction of NWs on the  $\alpha$ -plane quartz. The arrows show the crystallographic growth direction and orientation of  $\text{VO}_2$  rutile (110) planes with respect to the  $\alpha$ -plane quartz surface; (b) schematic of oxygen atoms in  $\alpha$ -plane quartz (large gray circles). The overlaid layer is V atoms (small red circles) and O atoms (Large navy-color circles) in  $\text{VO}_2$  rutile (110) plane. Figure 4b schematically simulates the SAED results: the parallelism of the (110) planes of  $\text{VO}_2$  rutile with the quartz  $\alpha$ -plane and the growth direction of NWs,  $(001)_{\text{rutile}}$ . Only with this arrangement will V atoms (small red circles) overlap with the Oxygen atoms of quartz (large gray circles).

the observed NW growth direction. In this figure, only V atoms which match with the oxygen atoms of the quartz are shown.

## Discussion

One-dimensional nanostructures such as carbon nanotubes, Si NWs, ZnO NWs, *etc.*, can receive a perfect control over diameter, density, position and orientation using the VLS growth mechanism with the appropriate metal catalysts and substrates<sup>23–25</sup>. In contrast, the thermal evaporation VS growth of  $\text{VO}_2$  NWs shows a poor controllability. Our work demonstrates that a special type of substrate, x-cut (11-20) quartz, facilitates the controlled growth of  $\text{VO}_2$  NWs at a lower cost, higher density, larger length, and better alignment. As revealed by prior experimental and theoretical studies, the nucleation rate is at its maximum when the fit between the lattices of nucleus and the substrate surface is at the highest<sup>26</sup>. Here, we also found that x-cut (11-20) quartz substrate can cause a much higher NW surface density than other lattice matched substrates though they also have a lattice fit relationship with  $\text{VO}_2$ . Thus, the nucleation and growth behavior of  $\text{VO}_2$  NWs is sensitive not only to the lattice match but also to the chemical identity of quartz substrates. This finding is consistent with the fact that the silicon dioxide surface favors the nucleation and growth of  $\text{VO}_2$  NWs<sup>15</sup>. In addition, the utilization of  $\text{V}_2\text{O}_5$  evaporation source provides a much higher vapor pressure because it has a much lower melting point of  $690^\circ\text{C}$  than that of  $\text{VO}_2$  ( $1967^\circ\text{C}$ ). As a result, the combination of the x-cut (11-20) quartz surface and  $\text{V}_2\text{O}_5$  provides an excellent seeding and fast

growth environment. Strelcov *et al.* has shown that silicon dioxide-based substrates, especially quartz, favor a high aspect ratio growth<sup>15</sup>. In our case, the competitive growth of NWs with a superior high nucleation density suppresses the elongation of NWs by physically stopping the growth fronts, as observed in Figs. 1c and 2b, leading to the NW's aspect ratio of less than 50. Our work advances a rational growth of  $\text{VO}_2$  NWs with regards to cost, orientation and surface density while the control over diameter, position and aspect ratio still remains a challenge and needs further investigations.

In conclusion, we report the horizontally aligned and dense growth mode for  $\text{VO}_2$  NWs on the polished x-cut quartz surface using a simple vapor transport method. It is shown that the product morphology ranges from MPs to NWs depending on the deposition temperature. The growth direction of NWs is along the  $[1-100]_{\text{quartz}}$  direction as identified by the HRTEM and SAED observations. Here, the self-assembly of  $\text{VO}_2$  NWs is attributed to an epitaxial crystal growth on the naked crystal plane of x-cut quartz. The combination of the low-melting-point source  $\text{V}_2\text{O}_5$  and lattice matched quartz substrates greatly facilitates the nucleation and enhances the growth rate. This approach is potentially a means for self-alignment of  $\text{VO}_2$  NWs in the lithography industry to design novel metal-insulator transition devices based on  $\text{VO}_2$  NWs such as near infrared linear polarizers<sup>27</sup> and microactuators<sup>8</sup>.

## Methods

$\text{VO}_2$  NWs were grown using a simple vapor transport method in which  $\text{V}_2\text{O}_5$  powder was placed in a quartz boat at the center of a horizontal tube furnace as seen in Fig. 1a. Argon (Ar) gas flow transported the V/O atoms to the quartz substrate where crystal growth took place. The reaction product was collected on the substrate which was placed close to the source quartz boat at the downstream location (Substrate is shown in Fig. 1a). The growth was carried out in the following condition: evaporation temperature  $\sim 880^\circ\text{C}$ , Ar carrier gas flow rate  $\sim 6.8$  sccm (standard-state cubic centimeter per minute), pressure  $\sim 5$  torr, and evaporation time  $\sim 2$  hours or more. We observed a distinct  $\text{VO}_2$  growth direction on x-cut quartz, which resulted in the growth of NWs on the basal plane of the substrate in a direction. The horizontal growth is shown to be highly dependent on the orientation of used quartz substrates: only x-cut polished quartz offers a high-density, oriented growth while polished quartz with other orientations gives randomly dispersed NWs growth embedded in the substrates as reported previously. The size distribution, lattice structure and crystal orientation of the as-synthesized products were characterized by optical microscopy (CASCADE CMPS-888L), scanning electron microscopy (SEM, Quanta 3D FEG), x-ray diffraction (XRD, Siemens D5000), and transmission electron microscopy (TEM, FEG CM200), as well as a Raman spectroscopy (INVIA, using a 488 nm Ar ion laser).

1. Eyert, V. The metal-insulator transitions of  $\text{VO}_2$ : A band theoretical approach. *Ann Phys. (Berlin, Ger.)* **11**, 650–702 (2002).
2. Fu, D. *et al.* Comprehensive study of the metal-insulator transition in pulsed laser deposited epitaxial  $\text{VO}_2$  thin films. *J. Appl. Phys.* **113**, 043707 (2013).
3. Cao, J. & Wu, J. Strain effects in low-dimensional transition metal oxides. *Mater. Sci. Eng. R Reports* **71**, 35–52 (2011).
4. Wu, C., Feng, F. & Xie, Y. Design of vanadium oxide structures with controllable electrical properties for energy applications. *Chem. Soc. Rev.* **42**, 5157–83 (2013).
5. Lee, S. *et al.* Axially engineered metal-insulator phase transition by graded doping  $\text{VO}_2$  nanowires. *J. Am. Chem. Soc.* **135**, 4850–5 (2013).
6. Cheng, C. *et al.* Heat transfer across the interface between nanoscale solids and gas. *ACS Nano* **5**, 10102–7 (2011).
7. Parikh, P. *et al.* Dynamically tracking the strain across the metal-insulator transition in  $\text{VO}_2$  measured using electromechanical resonators. *Nano Lett.* **13**, 4685–9 (2013).
8. Wang, K. *et al.* Performance limits of microactuation with vanadium dioxide as a solid engine. *ACS Nano* **7**, 2266–72 (2013).
9. Guo, J. *et al.* Nature of the metal insulator transition in ultrathin epitaxial vanadium dioxide. *Nano Lett.* **13**, 4857–4861 (2013).
10. Wei, J., Ji, H., Guo, W., Nevidomskyy, A. H. & Natelson, D. Hydrogen stabilization of metallic vanadium dioxide in single-crystal nanobeams. *Nano Lett.* **12**, 357–362 (2012).
11. Park, J. H. *et al.* Measurement of a solid-state triple point at the metal-insulator transition in  $\text{VO}_2$ . *Nature* **500**, 431–4 (2013).
12. Baik, J. M. *et al.* Pd-sensitized single vanadium oxide nanowires: highly responsive hydrogen sensing based on the metal-insulator transition. *Nano Lett.* **9**, 3980–4 (2009).
13. Hu, B. *et al.* External-strain induced insulating phase transition in  $\text{VO}_2$  nanobeam and its application as flexible strain sensor. *Adv. Mater.* **22**, 5134–9 (2010).



14. Cheng, C., Liu, K., Xiang, B., Suh, J. & Wu, J. Ultra-long, free-standing, single-crystalline vanadium dioxide micro/nanowires grown by simple thermal evaporation. *Appl. Phys. Lett.* **100**, 103111 (2012).
15. Strelcov, E., Davydov, A. V., Lanke, U., Watts, C. & Kolmakov, A. In situ monitoring of the growth, intermediate phase transformations and templating of single crystal VO<sub>2</sub> nanowires and nanoplatelets. *ACS Nano* **5**, 3373–84 (2011).
16. Kim, I. S. & Lauhon, L. J. Increased Yield and Uniformity of Vanadium Dioxide Nanobeam Growth via Two-Step Physical Vapor Transport Process. *Cryst. Growth Des.* **12**, 1383–1387 (2012).
17. Guiton, B. S., Gu, Q., Prieto, A. L., Gudixsen, M. S. & Park, H. Single-crystalline vanadium dioxide nanowires with rectangular cross sections. *J. Am. Chem. Soc.* **127**, 498–9 (2005).
18. Cheng, Y., Wong, T. L., Ho, K. M. & Wang, N. The structure and growth mechanism of VO<sub>2</sub> nanowires. *J. Cryst. Growth* **311**, 1571–1575 (2009).
19. Tselev, A. *et al.* Interplay between ferroelastic and metal-insulator phase transitions in strained quasi-two-dimensional VO<sub>2</sub> nanoplatelets. *Nano Lett.* **10**, 2003–11 (2010).
20. Strelcov, E., Davydov, A. V., Lanke, U., Watts, C. & Kolmakov, A. In situ monitoring of the growth, intermediate phase transformations and templating of single crystal VO<sub>2</sub> nanowires and nanoplatelets. *ACS Nano* **5**, 3373–84 (2011).
21. Xiang-Bai, C. Assignment of the raman modes of vo<sub>2</sub> in the monoclinic insulating phase. *J. Korean Phys. Soc.* **58**, 100 (2011).
22. Nikoobakht, B., Michaels, C. a., Stranick, S. J. & Vaudin, M. D. Horizontal growth and in situ assembly of oriented zinc oxide nanowires. *Appl. Phys. Lett.* **85**, 3244 (2004).
23. Zhu, C. *et al.* A self-entanglement mechanism for continuous pulling of carbon nanotube yarns. *Carbon N. Y.* **49**, 4996–5001 (2011).
24. Cheng, C. *et al.* Carbon-assisted nucleation and vertical growth of high-quality ZnO nanowire arrays. *AIP Adv.* **1**, 032104 (2011).
25. Cheng, C. *et al.* High-quality ZnO nanowire arrays directly fabricated from photoresists. *ACS Nano* **3**, 53–8 (2009).
26. Mithen, J. P. & Sear, R. P. Epitaxial nucleation of a crystal on a crystalline surface. *EPL* **105**, 18004 (2014).
27. Peng, X., Wang, B., Teng, J., Kana, J. B. K. & Zhang, X. Active near infrared linear polarizer based on VO<sub>2</sub> phase transition. *J. Appl. Phys.* **114**, 163103 (2013).

## Acknowledgments

Financial support from starting grants from South University of Science and Technology of China is gratefully acknowledged. The authors would like to thank Professor Junqiao Wu of the Department of Materials Science and Engineering, University of California, Berkeley, CA, USA and his laboratory for their kind support and for providing resources.

## Author contributions

C.C. designed the research, performed sample fabrication, analysed the results and wrote the paper. H.G., K. L., D.F. and J.Z. performed the TEM, the Raman, the XRD and AFM characterization and the paper revision. A.A. and H.S. incorporated in the interpretation of experimental results and final paper polishing.

## Additional information

**Competing financial interests:** The authors declare no competing financial interests.

**How to cite this article:** Cheng, C. *et al.* Self-Assembly and Horizontal Orientation Growth of VO<sub>2</sub> Nanowires. *Sci. Rep.* **4**, 5456; DOI:10.1038/srep05456 (2014).



This work is licensed under a Creative Commons Attribution-NonCommercial-NoDerivs 4.0 International License. The images or other third party material in this article are included in the article's Creative Commons license, unless indicated otherwise in the credit line; if the material is not included under the Creative Commons license, users will need to obtain permission from the license holder in order to reproduce the material. To view a copy of this license, visit <http://creativecommons.org/licenses/by-nc-nd/4.0/>